J Arid Land (2024) 16(5): 632–653
https://doi.org/10.1007/s40333-024-0015-1

Science Press Springer-Verlag

Grain size and surface micro-texture characteristics and their paleoenvironmental significance of Holocene sediment in southern margin of the Gurbantunggut Desert, China

MA Yunqiang[1,2], LI Zhizhong[1,2,3*], TAN Dianjia[1,2], ZOU Xiaojun[1,2], TAO Tonglian[1,2]

[1] School of Geographical Sciences, Fujian Normal University, Fuzhou 350117, China;
[2] Key Laboratory for Humid Subtropical Eco-geographical Processes of the Ministry of Education, Fujian Normal University, Fuzhou 350117, China;
[3] Institute of Geography, Fujian Normal University, Fuzhou 350117, China

Abstract: The southern margin of the Gurbantunggut Desert, China, is characterized by alternating layers of aeolian and alluvial deposits. Investigating the characteristics of arenaceous sediment in this area is of significant importance for understanding the interactive processes of wind and water forces, as well as the provenance of sediment. However, there are relatively few investigations on the characteristics of such sediment at present. In this study, we researched three aeolian-alluvial interactive stratigraphic profiles and different types of surface sediment on the desert-oasis transitional zone of southern margin of the Gurbantunggut Desert. Based on the optically stimulated luminescence (OSL) dating of aeolian sand and analyses of quartz sand grain size and surface micro-texture, we explored the aeolian-alluvial environmental change at southern margin of the desert in Holocene, as well as the provenance of sediment. The results indicated that the grain size characteristics of different types of sediment in the stratigraphic profiles were similar to those of modern dune sand, interdune sand, muddy desert surface soil, and riverbed sand. Their frequency curves were unimodal or bimodal, and cumulative probability curves were two-segment or three-segment, mainly composed of suspension load and saltation load. The quartz sand in the sediment at southern margin of the desert had undergone alternating transformation of various exogenic forces, with short transportation distance and time, and sedimentary environment was relatively humid. In Holocene, southern margin of the desert primarily featured braided river deposits, and during intermittent period of river activity, there were also aeolian deposits such as sand sheet deposits, stabilized dune deposits, and mobile dune deposits. The provenance for Holocene alluvial deposits at southern margin of the desert remains relatively constant, with the debris of the Tianshan Mountains being the primary provenance. Aeolian sand is mainly near-source recharge, which is formed by *in situ* deposition of fluvial or lacustrine materials in southern margin of the desert transported by wind erosion, and its provenance was still the weathered debris of the Tianshan Mountains. In addition, the sand in interior of the desert may be transported by northwest wind in desert-scale, thus affecting the development of dunes in southern margin of the desert. The results of this study provide a reference for understanding the composition and provenance changes of desert sand in the context of global climate change.

Keywords: aeolian-alluvial deposition; grain size; surface micro-texture; sedimentary environment; Holocene

Citation: MA Yunqiang, LI Zhizhong, TAN Dianjia, ZOU Xiaojun, TAO Tonglian. 2024. Grain size and surface micro-texture characteristics and their paleoenvironmental significance of Holocene sediment in southern margin of the Gurbantunggut Desert, China. Journal of Arid Land, 16(5): 632–653. https://doi.org/10.1007/s40333-024-0015-1

*Corresponding author: LI Zhizhong (E-mail: lizz@fjnu.edu.cn)
Received 2023-11-18; revised 2024-03-29; accepted 2024-04-19
© Xinjiang Institute of Ecology and Geography, Chinese Academy of Sciences, Science Press and Springer-Verlag GmbH Germany, part of Springer Nature 2024

1 Introduction

As significant geographical unit in arid and semi-arid areas, desert is the product of the interaction of various factors such as landform, climate, and hydrology (Lancaster, 1995; Pye and Tsoar, 2009). The formation and development of desert has a significant impact on the evolution of regional land surface process and even global climate change (Goudie and Middleton, 2006; Yang et al., 2012). The edge of desert exists within the zone of interaction among various surface layers (Yang and Eitel, 2016), where exogenic forces are active. Typically, the sedimentary strata in these areas consist of alternating aeolian and alluvial sequences (Goudie, 2002; Parsons and Abrahams, 2009), making them ideal materials for reconstructing desert paleoenvironment. Therefore, understanding the characteristics of aeolian-alluvial sediment at the margin of desert is of significant importance for comprehending the processes of exogenic force interaction and tracing sand provenance.

Grain size is a fundamental characteristic for sediment, which is used to measure the transport medium and energy, reflecting the deposition process and sand provenance (Team Northern Shannxi of Chengdu Institute of Geology (TNSCIG), 1978). Quartz sand is widely distributed, relatively hard, and chemically stable. However, it is influenced by mechanical abrasion and chemical dissolution in different environments, retaining distinct micro-texture on its surface. The micro-texture makes it widely applicable in the study of paleoenvironment (Krinsley and Doornkamp, 1973; Dai, 1988). Therefore, comprehensive analysis of grain size and surface micro-texture of quartz sand contributes to a deeper exploration of the sedimentary environmental change at the margin of desert and sand provenance.

The Gurbantunggut Desert, with an approximate area of 5.63×10^4 km^2, is the second largest desert in China (Zhu et al., 1980). Previous research has extensively investigated the grain size and surface micro-texture characteristics of sediment in interior of the desert and surrounding areas, leading to valuable insights into sedimentary environment and sand provenance of the desert. For instance, Huang and Zhou (2000) analyzed the characteristics of grain size and quartz sand in borehole sediment from the interdune in south of the desert, and observed significant variations in sand grain size and various features of wind, water, and chemical effects on the surface of quartz sand. Thus, three climate fluctuation events since late Pleistocene were identified. Shi and Xu (2007) studied the sand features of alluvial sediment in southern margin of the desert using grain size analysis and scanning electron microscope, and found that its grain composition resembled dune sand, with poorly rounded quartz sand and widespread traces of aeolian and fluvial erosion. They suggested that alluvial plain at southern margin of the desert experienced aeolian deposition during dry climate period in Holocene. Huang (1996) and Qian and Wu (2010) investigated the sand features in borehole sediment in the north and south of the desert. Results indicated that sandy sediment in Holocene had finer grains and better sorting, with more pronounced traces of glacial, fluvial, and chemical effects on quartz sand surface. Recent studies on the surface sand characteristics in the Gurbantunggut Desert also showed that dune sand in southern margin of the desert was notably influenced by wind-driven sorting, and tended to be finer, exhibiting significant mechanical and chemical effects on the surface of quartz sand and boasting a rich variety of sand provenance (Liu, 2020; Zhao, 2020; Zhu et al., 2021; Gao et al., 2022a).

In light of preceding studies, it is evident that current researches on the sand characteristics of the Gurbantunggut Desert in Holocene are relatively few, and the results are focus on single surface sediment or stratigraphic sediment, lacking comparative studies of those results. Furthermore, southern margin of the Gurbantunggut Desert, adjacent to the Tianshan Mountains, is significantly affected by wind and water effects in the transition zone between desert and oasis. The sedimentary environment is unique and the sand provenance is complex. There are few studies revealing the dynamic changes of sedimentary environment and sand provenance at southern margin of the desert through aeolian and alluvial stratigraphic sediment characteristics. Given these circumstances, we systematically studied the characteristics of grain size and quartz

sand surface micro-textures of Holocene sediment in southern margin of the Gurbantunggut Desert, in order to reveal Holocene sedimentary environmental change and sand provenance, and to provide a scientific basis for predicting the long-term trend of desertification in the study area.

2 Study area

The study area is situated at the convergence of the Gurbantunggut Desert and the alluvial plain in northern piedmont of the Tianshan Mountains, China (Fig. 1). The Junggar Basin is deeply nestled within the Asian continent, with a blocked terrain, which is higher in the northeast and lower in the southwest (Wu, 1962). The Gurbantunggut Desert within it is significantly influenced by westerly circulation, boasting relatively good vegetation coverage, and being the largest fixed and semi-fixed desert in China (Chen, 1963; Zhu et al., 1980; Wu, 2009). The desert belongs to a temperate continental arid climate with an average annual precipitation of 120 mm and an annual average temperature ranging from 4℃ to 7℃ (Yang et al., 2004; Qian and Wu, 2010). Due to the unique topographical layout, the westerlies enter the basin from western Alataw Pass, the Emin River valley, and the northern Irtix River valley (Xinjiang Expedition of Chinese Academy of Sciences (XECAS), 1978; Yin, 1987), forming west and northwest wind near the surface (Fig. 1). Surface water is scarce in the study area, with most rivers originating from the Tianshan Mountains, being fed by glacial meltwater (Qian and Wu, 2010). These rivers run parallel, converging at the margin of the desert (Li et al., 2020), carrying debris resulting from glacial abrasion and frost weathering to form alluvial plains (XECAS, 1978; Zhu et al., 1980). In low-lying areas, the water accumulates into lakes, forming shallow wetlands and marshes (Zhu et al., 1980). The desert hosts a diverse range of plant species, with higher vegetation coverage on gentle dunes slopes and interdunes (Chen, 2010; Qian and Wu, 2010). Vegetation coverage is relatively poorer on the top of dunes, forming the primary areas for wind erosion and accumulation.

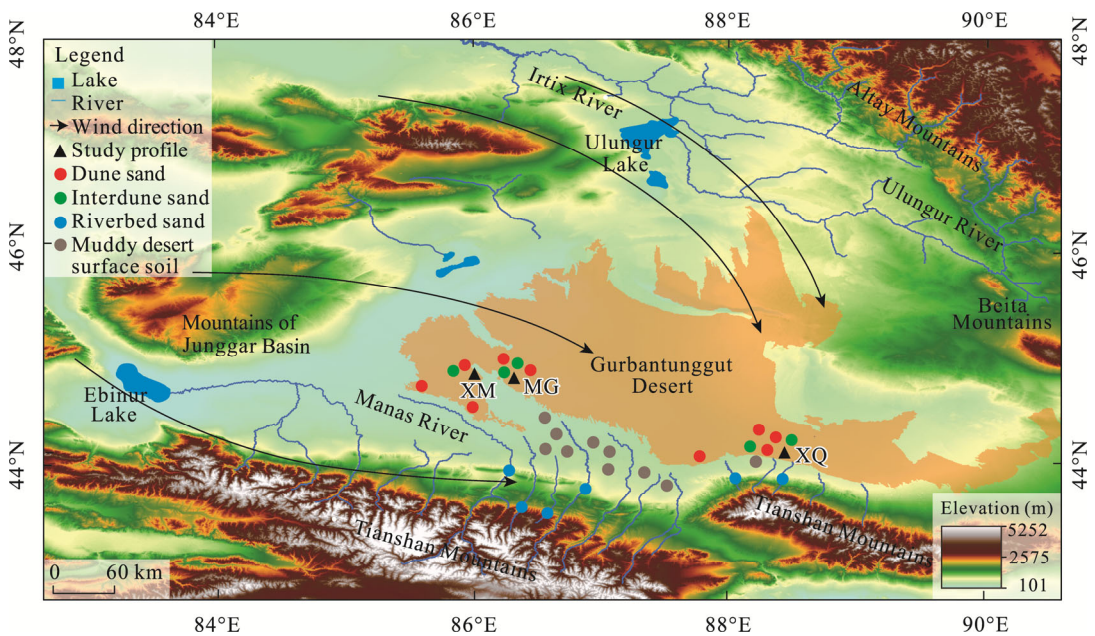

Fig. 1 Overview of the study area and sampling locations. XM, MG, and XQ are three study profiles.

3 Materials and methods

3.1 Profile overview and sample collection

The study profiles are located in the transitional zone between southern margin of the

Gurbantunggut Desert and the oasis (Fig. 1). Sedimentary sequences of study profiles are primarily composed of alternating alluvial and aeolian layers, with aeolian dunes covering the top. Lithologic characteristics of each profile are shown in Table 1. Totally three profiles are selected, i.e., MG, XM, and XQ profiles. MG profile (45°03′16″N, 86°14′06″E), with a thickness of 365 cm, consists of diluvial deposits, floodplain deposits, and aeolian deposits (Fig. 2a). XM profile (45°07′19″N, 85°58′23″E), with a thickness of 355 cm, consists of floodplain deposits, diluvial deposits, stabilized dune deposits, and mobile dune deposits (Fig. 2b). XQ profile (44°25′44″N, 88°22′26″E), with a thickness of 425 cm, consists of aeolian deposits, diluvial deposits, limnic deposits, and riverbed deposits (Fig. 2c).

Table 1 Lithologic characteristics of study profile

Profile	Depth (m)	Color	Granularity	Structure
MG	0–70	Reddish-brown	Silty clay	Massive structure
	70–130	Reddish-brown, pale-yellow	Silty clay, silt	Massive structure
	130–185	Grey-yellow	Very fine sand	Cross-bedding
	185–295	Grey-yellow, reddish-brown	Very fine sand, silty clay	Horizontal bedding
	295–365	Reddish-brown	Silty clay	Massive structure
XM	0–30	Light-yellow	Clayish silt	Wavy bedding
	30–115	Reddish-brown	Silty clay	Massive structure
	115–145	Light-gray	Silt	Horizontal bedding
	145–240	Light-green	Silt	Asymmetrical ripple, cross-bedding
	240–355	Gray	Fine sand	Cross-bedding
XQ	0–142	Dark-yellow, purple-red	Very fine sand, clayish silt	Horizontal bedding, massive structure
	142–305	Gray-green	Silt	Sandy iron-manganese rusty spot
	305–425	Gray	Fine sand	Trough cross-bedding

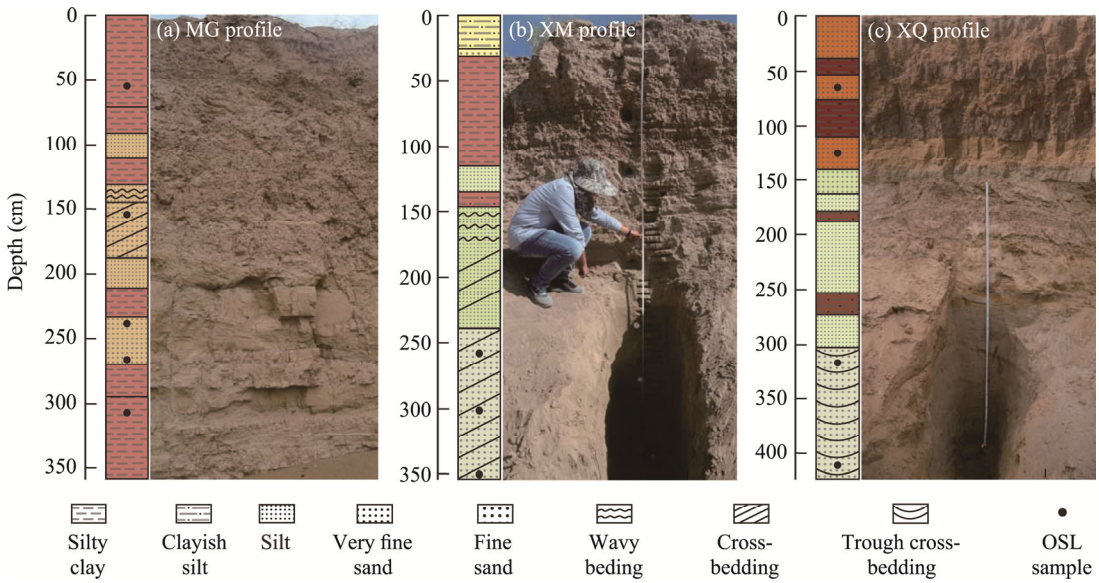

Fig. 2 Photos and lithological columns of study profiles. (a), MG profile; (b), XM profile; (c), XQ profile. OSL, optically stimulated luminescence.

Given that optically stimulated luminescence (OSL) dating technology has the best effect on aeolian sand (Aitken, 1998; Stokes et al., 2004; Robins et al., 2021), OSL dating samples were

collected under dark conditions in aeolian sand layers after removing surface weathering materials from the profiles (Lai and Ou, 2013). Environmental proxy samples were collected at irregular intervals ranging from 5 to 10 cm apart, totaling 166 samples across the three profiles. Building upon on-the-spot investigation and considering the natural geographical characteristics of the study area, we collected different types of surface sediment from southern margin of the Gurbantunggut Desert and northern piedmont of the Tianshan Mountains, totaling 30 samples. The main sand types included dune sand, interdune sand, muddy desert surface soil, and riverbed sand (Fig. 1).

3.2 Methods

3.2.1 OSL dating

The equivalent dose (D_e) testing of OSL dating samples from XM profile was carried out at the Luminescence Dating Laboratory, School of Geographical Sciences, Fujian Normal University, China. D_e was determined using the single aliquot regenerative-dose (SAR) protocol (Murray and Wintle, 2000; Wintle and Murray, 2006), and measurements were made using Danish Risø luminescence reader (TL/OSL-DA-20C/D, DTU Nutech, Kongens Lyngby, Denmark). After pretreatment, we sent the samples to China Institute of Atomic Energy for the measurement of uranium (U), thorium (Th), and kalium (K) contents using neutron activation analysis. Water content of the samples was measured approximately 5%, and we calculated the contribution of cosmic rays based on the sample's latitude, altitude, and burial depth, following Prescott and Hutton (1994). Environmental dose rate (D) of the samples was estimated accordingly. Burial age of the samples was determined using age calculation formula: age (a)=equivalent dose (D_e)/environmental dose rate (D).

OSL dating of MG and XQ profiles was conducted at the Luminescence Dating Laboratory of the Institute of Crustal Stress, China Earthquake Administration. For MG profile, samples MG1, MG3, MG4, and MG5 used 4–11 μm fine quartz grains and were dated using simple multi-aliquot regenerative-dose (SMAR) protocol (Wang and Lu, 2005) to obtain D_e. Sample MG2 and samples XQ1–XQ4 selected 90–125 μm coarse quartz grains and were dated using SAR procedure to determine D_e.

3.2.2 Grain size analysis

Grain size analysis was conducted using the laser diffraction particle size analyzer (Mastersizer 2000, Malvern Instruments, Malvern, UK) at the School of Geographical Sciences, Fujian Normal University, China. The range of instrument spans from 0.02 to 2000.00 μm. Prior to testing, we carried out repeatability tests, with measurement errors less than 1%. Grain size of the sediment was represented using Φ value ($\Phi = -\log_2 D'$, where D' is the grain size in mm). We categorized the grain size classes based on the Udden-Wentworth standard, as follows: gravel (< –1 Φ), very coarse sand (–1–0 Φ), coarse sand (0–1 Φ), medium sand (1–2 Φ), fine sand (2–3 Φ), very fine sand (3–4 Φ), silt (4–9 Φ), and clay (>9 Φ). Mean grain size, sorting, skewness, and kurtosis were calculated using the Folk-Ward graphic method formula (Folk and Ward, 1957). Additionally, a granulometric end-member (EM) analysis was performed on the stratigraphic sediment using the algorithm proposed by Paterson and Heslop (2015).

3.2.3 Surface micro-texture of quartz sand analysis

The observation of quartz sand morphology and surface micro-texture was conducted at the School of Geographical Sciences, Fujian Normal University, China, using the scanning electron microscope (JCM-6000Plus, JEOL, Tokyo, Japan). This study involved the observation and statistical analysis of the morphology and surface micro-texture of a total of 992 quartz particles, comprising 13 stratigraphic samples and 12 surface samples. We carried out the statistical analysis of quartz sand morphology and roundness according to the method proposed by Powers (1953), while the classification and interpretation of surface micro-texture followed the method presented by Krinsley and Doornkamp (1973).

4 Results

4.1 Chronostratigraphy

Ages of OSL dating samples from the study profiles are presented in Table 2. For most samples, OSL ages were consistent with the stratigraphic sequences, except for a slight inversion observed in the bottom alluvial layer samples from MG profile. Age reversal may be attributed to the difference of *D* caused by the mineral composition. Compared with MG3 and MG4, *D* of MG5 was high (Table 2). XM and MG profiles at southwestern margin of the desert represented mid to late Holocene deposits dating back to approximately 5.0 ka. The bottom sand layer in XQ profile (at 4.25 m below the surface) had an OSL age of approximately 11.1 ka, indicating early Holocene sedimentation. In summary, these three profiles provided records of environmental information in southern margin of the desert since Holocene.

Table 2 Chronology and related parameters of the OSL (optically stimulated luminescence) dating samples in study profiles

Sample number	Depth (m)	U (μg/g)	Th (μg/g)	K (μg/g)	Water content (%)	Grain size (μm)	Procedure	*D* (Gy/ka)	D_e (Gy)	Age (ka)
XM1	2.60	1.44±0.05	5.47±0.05	2.08±0.01	5±1	63–125	SAR	2.78±0.04	12.95±4.17	4.66±1.50
XM2	3.00	1.37±0.05	4.74±0.05	2.06±0.01	5±1	63–125	SAR	2.71±0.04	13.04±3.19	4.82±1.18
XM3	3.50	1.43±0.05	4.98±0.05	2.09±0.01	5±1	63–125	SAR	2.77±0.04	13.81±1.30	4.99±0.47
MG1	0.55	3.57±0.04	12.3±0.15	2.45±0.02	5±5	4–11	SMAR	5.04±0.37	8.74±0.40	1.73±0.15
MG2	1.55	2.54±0.05	9.52±0.09	2.07±0.02	5±5	90–125	SAR	3.34±0.14	8.15±0.18	2.44±0.12
MG3	2.50	2.27±0.04	7.78±0.15	2.06±0.02	5±5	4–11	SMAR	3.72±0.28	9.06±0.39	2.43±0.21
MG4	2.75	2.57±0.04	8.50±0.16	2.05±0.02	5±5	4–11	SMAR	3.88±0.29	9.33±0.20	2.41±0.19
MG5	3.10	3.52±0.10	11.6±0.30	2.24±0.01	5±5	4–11	SMAR	4.69±0.35	10.53±0.85	2.25±0.25
XQ1	0.66	1.51±0.01	7.78±0.10	1.91±0.02	5±5	90–125	SAR	2.87±0.12	11.48±0.76	4.01±0.31
XQ2	1.26	1.24±0.01	5.25±0.09	2.01±0.01	5±5	90–125	SAR	2.72±0.11	15.65±1.06	5.76±0.46
XQ3	3.25	1.02±0.01	3.51±0.02	1.63±0.02	5±5	90–125	SAR	2.14±0.09	23.08±0.80	10.79±0.59
XQ4	4.05	0.94±0.01	3.02±0.03	1.75±0.01	5±5	90–125	SAR	2.19±0.09	24.32±1.27	11.11±0.75

Note: U, uranium; Th, thorium; K, kalium; SAR, single aliquot regenerative-dose; SMAR, simple multi-aliquot regenerative-dose; *D*, environmental dose rate; D_e, equivalent dose. Mean±SE.

4.2 Grain size characteristics

4.2.1 Surface sediment

Different types of surface sediment in the study area exhibited a wide range of grain size distribution and significant difference in grain size composition (Fig. 3). Muddy desert surface soil had the finest grain size, with the highest proportion of silt, followed by clay and very fine sand, along with some components of fine sand and medium sand. Interdune sediment was dominated by silt, with significant portions of very fine sand, fine sand, and clay, and a lower content of medium sand. Dune sand was characterized by a predominance of fine sand, medium sand, and very fine sand, with very low contents of coarse sand, silt, and clay. Riverbed sediment displayed substantial internal variations, with most samples ranging from silt to coarse sand, and a relatively higher content of fine sand and medium sand.

As shown in Figure 4a, the frequency curves of dune sand displayed a unimodal distribution with a peak around 2.00–3.00 Φ. Most of curves were sharp, with a few displaying slightly flatter profile. Interdune sand showed a bimodal distribution with a narrow primary peak around 3.00–4.00 Φ and a broader secondary peak ranging from 8.00 to 9.00 Φ (Fig. 4b). Muddy desert surface soil exhibited a polymodal distribution with significant internal variability. There were two main patterns (Fig. 4c): one was bimodal with a sharp primary peak around 4.00–5.00 Φ and a distinct fine tail, while the secondary peak was less prominent with a peak around 1.00 Φ. The

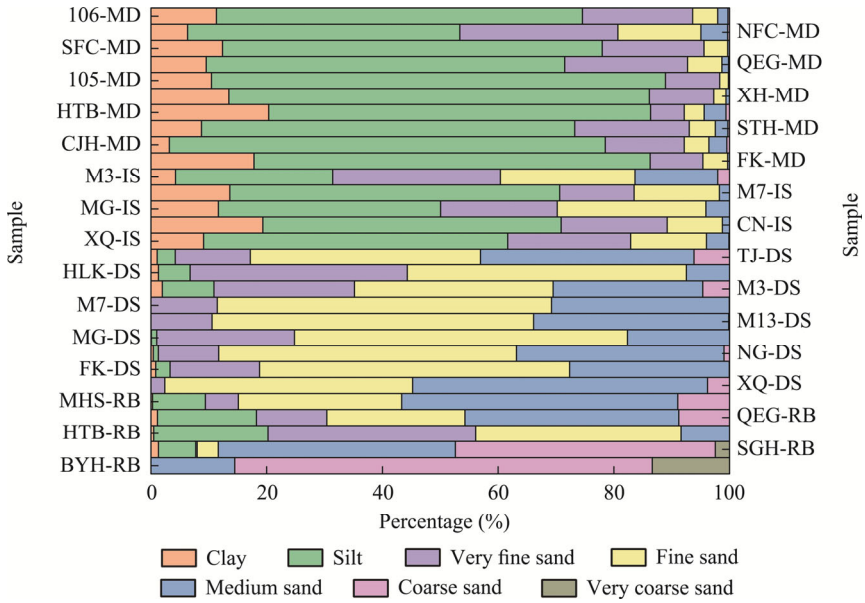

Fig. 3 Grain size composition of different types of surface sediment from DS, IS, MD, and RB. DS, dune sand; IS, interdune sand; MD, muddy desert surface soil; RB, riverbed sand. The abbreviations are the same in the following figures.

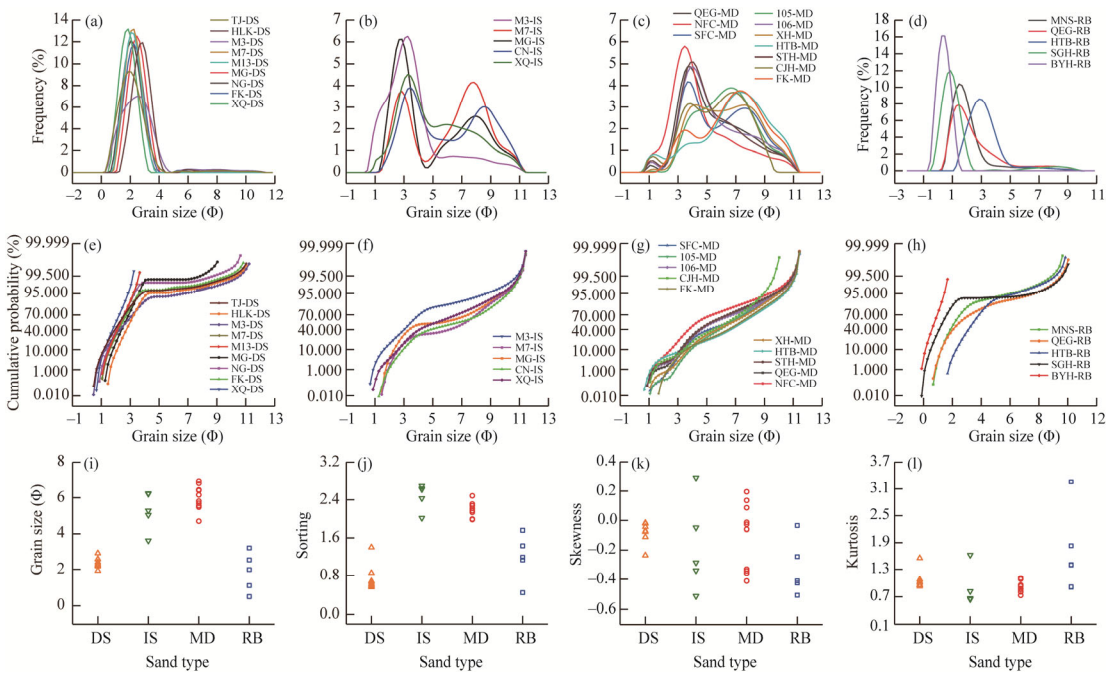

Fig. 4 Frequency curves (a–d), cumulative probability curves (e–h), and granulometric parameters (i–l) of different types of surface sediment from DS, IS, MD, and RB

other pattern was trimodal with both the primary and secondary peaks being relatively flat, forming a saddle-shaped distribution. Riverbed sand showed a unimodal distribution, and most of the samples had peaks ranging from 0.00 to 2.00 Φ, although there were some variations between individual samples (Fig. 4d).

In terms of cumulative probability curves in dune sand (Fig. 4e), except for samples of M13-DS and XQ-DS, which consisted of a single segment (saltation load), the remaining samples were two-segment. They were primarily composed of saltation load with a small amount of

suspension load. Interdune sand (Fig. 4f) also exhibited a two-segment pattern, with a significant proportion of suspension load and a corresponding reduction in saltation load. Surface soil in muddy desert displayed a distinct inflection point at the beginning (Fig. 4g), corresponding to the third peak in the frequency curve. This result indicated the presence of a small amount of coarse traction load. Riverbed sand (Fig. 4h) also displayed a two-segment pattern, with the saltation load being dominant, and the suspension load was higher than that in dune sand.

As shown in Figure 4i, the mean grain size of surface sediment decreased from riverbed sand, dune sand, interdune sand to muddy desert surface soil. About sorting, dune sand exhibited good sorting with values ranging from 0.56 to 1.40 (Fig. 4j). Interdune sand and muddy desert surface soil showed poorer sorting with values ranging from 2.00 to 3.00. Riverbed sand sorting was inferior to dune sand, with values ranging from 0.44 to 1.76. In terms of skewness, dune sand displayed a slight positive skewness, with skewness values ranging from –0.23 to –0.01 (Fig. 4k). Interdune sand and muddy desert surface soil generally exhibited negative skewness, with skewness values ranging from –0.51 to 0.19. Riverbed sand skewness values ranged from –0.51 to –0.03, indicating a marked negative value. Regarding kurtosis, dune sand exhibited moderate kurtosis, with kurtosis values ranging from 0.93 to 1.55 (Fig. 4l). Interdune sand and muddy desert surface soil generally had lower kurtosis values, with most samples ranging from 0.63 to 1.11, indicating a slightly flat kurtosis. Riverbed sand kurtosis values ranged from 0.91 to 3.26, indicating a sharp kurtosis.

4.2.2 Stratigraphic sediment

Sediment grain size distribution within the study profiles was quite extensive, encompassing all grain size components from clay to coarse sand (Fig. 5). MG profile was primarily composed of silt, with lower proportions of clay and very fine sand. Diluvial deposits exhibited the highest content of silt, followed by clay. In the aeolian sand layers, there was a notable increase in very fine sand and fine sand, particularly at the depth of 135–185 cm. In the upper section of XM profile (0–115 cm), both the floodplain deposits and diluvial deposits contained high content of silt and clay. In the middle section (115–240 cm), the components of very fine sand and fine sand significantly increased. Below 240 cm, there was a distinct increase in sediment grain size, even including component of coarse sand. XQ profile displayed coarser sediment compared with MG and XM profiles. While diluvial and limnic deposits contained higher content of clay and silt,

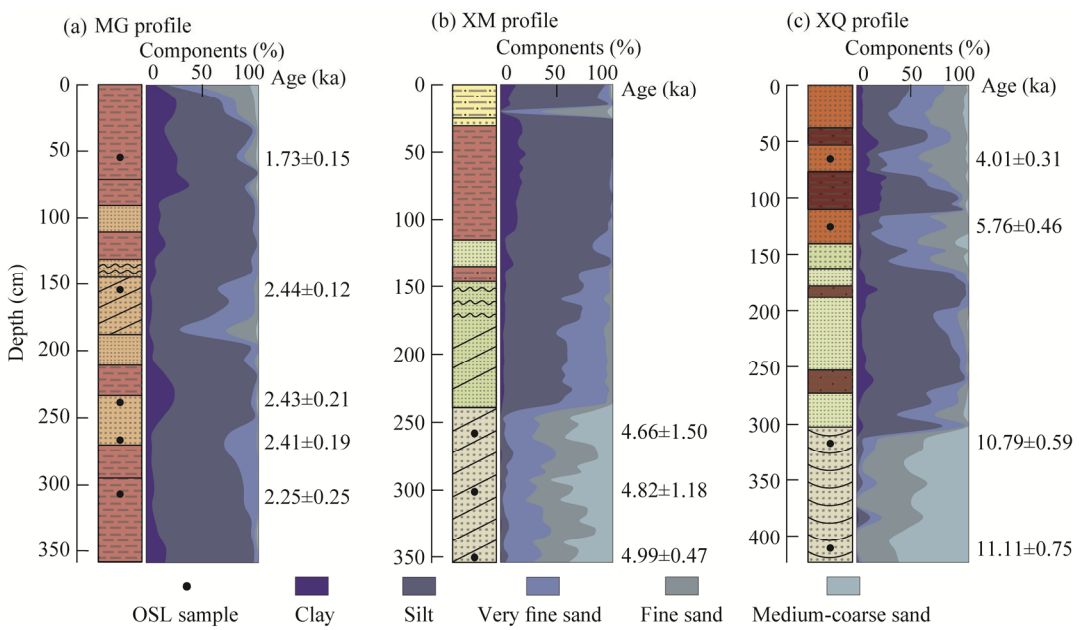

Fig. 5 Variations of grain size components of sediment with depth in study profiles. (a), MG profile; (b), XM profile; (c), XQ profile.

other layers contained proportions of components of silt. Particularly at the bottom of the profile, riverbed deposits (305–425 cm) exhibited a sudden increase in grain size, with a majority of particles composed of fine sand and medium to coarse sand.

We executed the AnalySize EM analysis in MATLAB to fit 10 potential granulometric EMs based on grain size data from each profile (Fig. 6). During the analysis, we determined the number of EMs for each profile based on linear correlation coefficient (R^2) and angular deviation. Generally, a higher R^2 (usually above 0.80) and a smaller angular deviation (usually less than 5) indicated a better fit by EMs. Following the principles of EM selection, the number of granulometric EMs for MG profile was determined to be 5 (Fig. 7a). Among them, EM1 and EM2 mainly dominated in diluvial deposits. EM3 was predominant in floodplain deposits, while EM4 and EM5 had higher proportions in aeolian deposits. A total of 5 granulometric EMs were extracted from XM profile (Fig. 7b). EM1 mainly existed in diluvial deposits. EM2 occurred in floodplain deposits. EM3 had a high content in stabilized dune deposits, while EM4 and EM5 accounted for a large proportion in mobile dune deposits. There were 6 granulometric EMs in XQ profile (Fig. 7c). EM1 dominated in diluvial deposits. EM2 and EM3 were abundant in limnic deposits. EM4 was predominant in aeolian deposits, while EM5 and EM6 were concentrated in riverbed deposits.

Plotting the granulometric EMs reveals significant differences in their grain size compositions (Fig. 8). In MG profile, EM1 exhibited the highest proportion of clay (67.98%). EM2 and EM3 contained a substantial amount of silt (78.88% for EM2 and 84.46% for EM3, respectively). EM4 displayed relatively high levels of silt (51.58%) and sand (45.44%), while EM5 comprised a significant amount of sand (82.78%). Within XM profile, EM1 was primarily composed of silt (59.46%) and clay (40.15%). EM2 contained a high proportion of silt (86.37%). EM3 still featured a predominant presence of silt (53.52%), but sand content (42.90%) had notably increased. EM4 and EM5 showed similar grain size compositions, with sand content reaching 97.08% and 97.88%, respectively. In XQ profile, EM1 exhibited the highest clay content

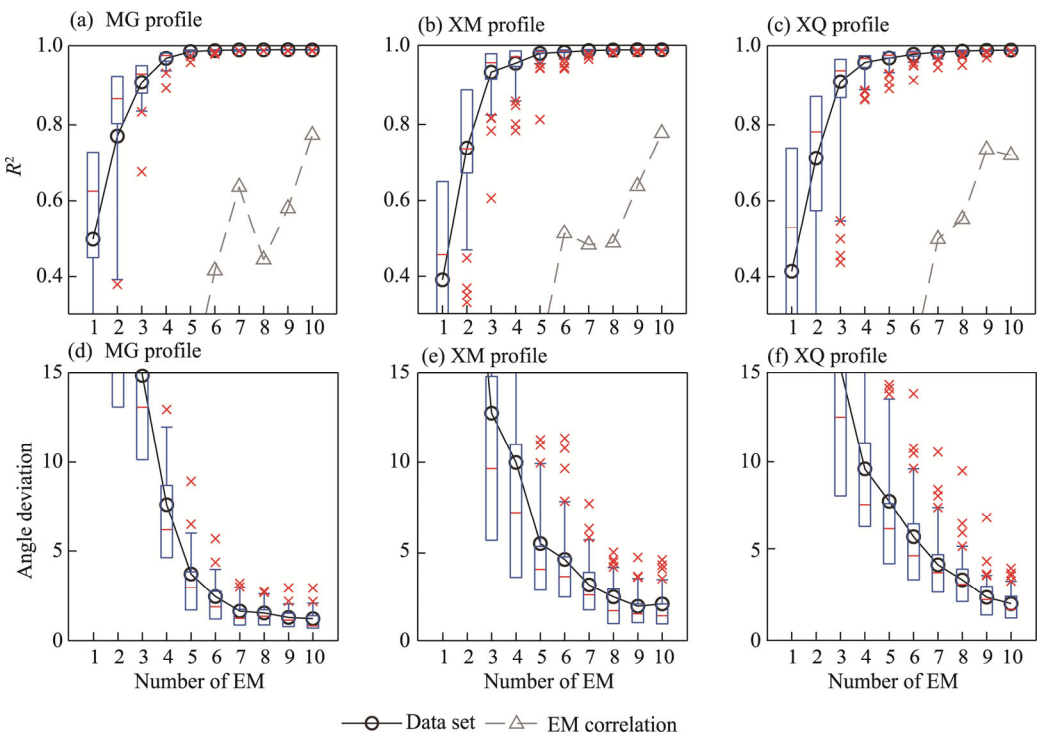

Fig. 6 Granulometric end-member (EM) analysis results of study profiles. (a)–(c) are linear correlation coefficients; (d)–(f) are angle deviations. Boxes indicate the IQR (interquartile range, 75th to 25th of the data). The median value is shown as a line within the box. Lines extend to the most extreme value within 1.5×IQR. Outlier is shown as whisker.

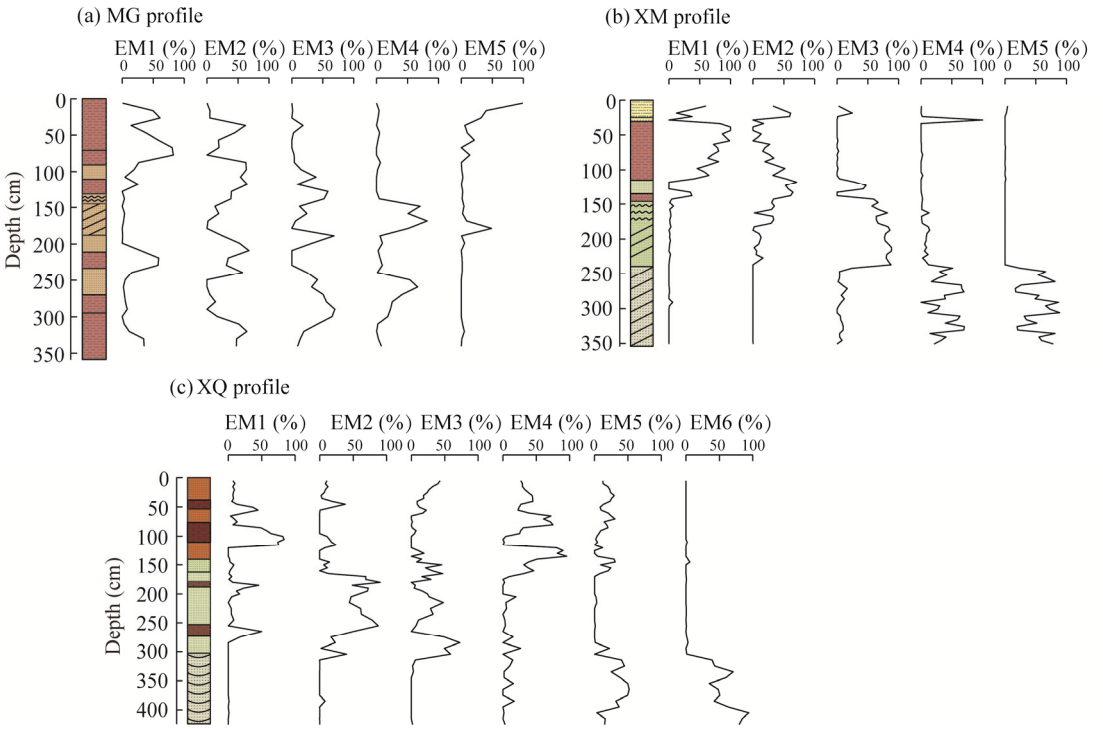

Fig. 7 Variations of EMs of sediment with depth in study profiles. (a), MG profile; (b), XM profile; (c), XQ profile.

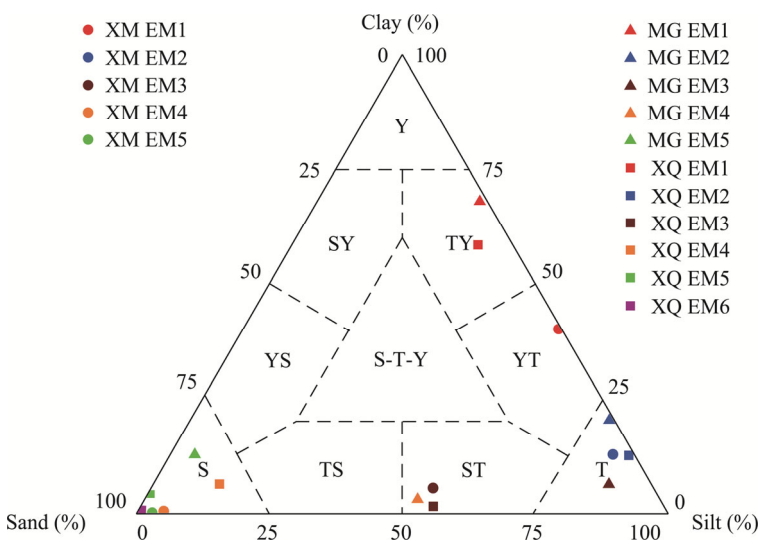

Fig. 8 Granulometric diagram of EMs in the study profiles. Y, clay; T, silt; S, sand; TY, silty clay; YT, clayish silt; ST, sandy silt; TS, silty sand; YS, clayish sand; SY, sandy clay.

(56.24%), followed by silt (34.82%). EM2 showed the highest proportion of silt (86.55%). EM3 displayed relatively equal proportions of silt (54.49%) and sand (44.08%). EM4, EM5, and EM6 showed a progressive increase in sand content (82.95%, 95.29%, and 99.35%, respectively), with a significant decrease in silt content (10.33%, 1.47%, and 0.65%, respectively) and clay content (6.72%, 3.24%, and 0.00%, respectively).

Frequency curves of EM1 in MG profile displayed a broad and gentle single peak (Fig. 9a). EM2 also showed a broad and gentle single peak, and the curve was coarse-skewed. EM3 was

bimodal, with a primary peak exhibiting normal distribution and a faint secondary peak. EM4 and EM5 shared a similar bimodal pattern, with sharper primary peaks and flat secondary peaks. Within XM profile, EM1 demonstrated a positively skewed, broad, and gentle single peak (Fig. 9b). EM2 displayed a nearly normal distribution but exhibited a notable fine tail. EM3 and EM4 shared similar curve shapes, featuring sharp primary peaks and less pronounced secondary peaks. EM5 showed a saddle-shaped double peak, with a wide span in the peak area. In XQ profile, EM1 displayed a bimodal distribution (Fig. 9c), with the primary peak showing a positively skewed wide peak. EM2 showed a broad and gentle single peak, slightly positively skewed. EM3 showed a positively skewed single peak, and EM4, EM5, and EM6 were similar in curve shapes, both featured by sharp single peak.

Cumulative probability curves of EM1 and EM2 in MG profile consisted of suspension, saltation, and traction loads (Fig. 9d), with suspension load exceeding 95.000%. EM3 and EM4 exhibited a three-segment distribution, where saltation load was above 85.000%. EM5 was two-segment distribution with saltation load representing about 80.000%. In XM profile, EM1 was composed of suspension, saltation, and traction loads (Fig. 9e), with suspension load accounting for over 99.000%. EM2 and EM3 both were three-segment distribution, with saltation load as the primary portion. EM4 was two-segment distribution, with saltation load exceeding 95.000%. EM5 consisted of saltation and traction loads, with each accounting for 50.000%. In XQ profile, EM1 followed a three-segment distribution (Fig. 9f), with high proportion of

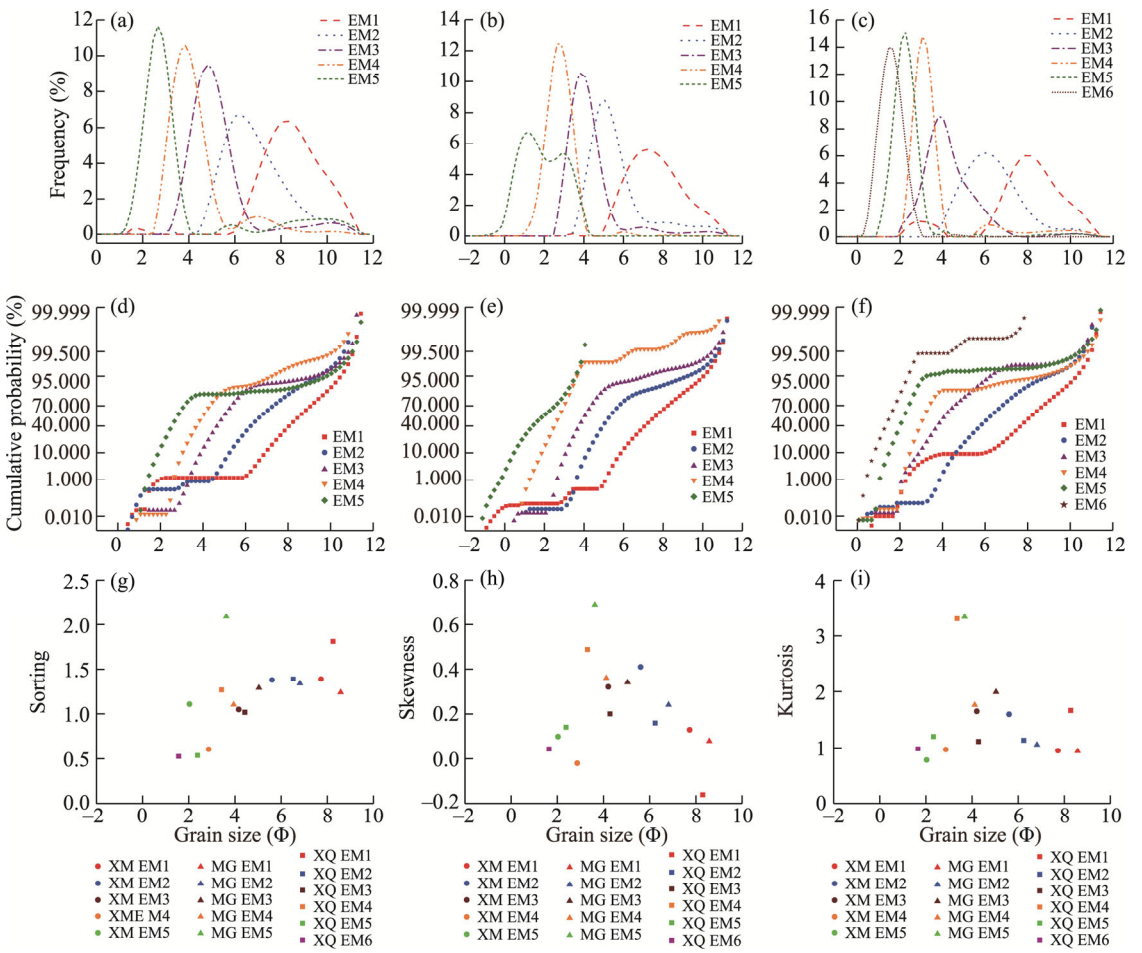

Fig. 9 Frequency curves (a–c), cumulative probability curves (d–f), and grain size parameters scatter plots (g–i) of EMs in MG, XM, and XQ profiles

suspension load. EM2 had saltation load representing more than 80.000%, followed by suspension and traction loads. EM3 was three-segment distribution, with saltation load exceeding 95.000%. EM4, EM5, and EM6 were composed of suspension and saltation loads, and saltation load gradually increased from EM4 to EM6.

Mean grain size of granulometric EMs ranged from 1.00 to 9.00 Φ (Fig. 9g), with most EMs falling between 4.00 and 9.00 Φ. Sorting of each EM varied between 0.50 and 2.10, only EM4 in XM profile, and EM5 and EM6 in XQ profile displayed relatively good sorting, with values lower than 0.71. As for skewness, except for EM1 in XQ profile showing negative skewness with a value lower than –0.10, most other EMs ranged from –0.10 to 0.70, exhibiting nearly symmetrical to positively skewed distribution (Fig. 9h). The kurtosis of EMs varied widely, with values between 0.90 and 3.50, and most EMs displaying sharp or normal distribution (Fig. 9i). Through scatter plots of granulometric parameters, it was evident that sorting of EMs and mean grain size showed a certain positive correlation (R^2=0.41). This result indicated that as sediment grain size increased, the sorting gradually improved. However, skewness (R^2= –0.06) and kurtosis (R^2=0.01) did not exhibit a significant correlation with mean grain size.

4.3 Morphology and surface micro-texture of quartz sand

4.3.1 Morphology and roundness

In surface sediment, the morphology of dune sand was predominantly circular (75.51%) and subrounded (46.00%) (Table 3). In comparison with dune sand, interdune sand had a higher percentage of square particles (35.29%). The particles were mainly subangular (32.00%) and angular (30.00%). Muddy desert surface soil had a higher content of square (34.00%) and rectangular (30.00%) sand, and angular (44.23%) particles were predominant. Square particles (44.55%) were more prominent, and angular particles (77.45%) overwhelmingly dominated in riverbed sand. Overall, the roundness of quartz sand in surface sediment followed the sequence from high to low: dune sand, interdune sand, muddy desert surface soil, and riverbed sand.

Table 3 Frequency of shape and roundness of quartz sand grains for surface sediment and stratigraphic sediment in study profiles

Sample type	Shape				Roundness			
	Circular (%)	Square (%)	Rectangular (%)	Triangular (%)	Rounded (%)	Subrounded (%)	Subangular (%)	Angular (%)
DS	75.51	14.29	8.16	2.04	22.00	46.00	24.00	8.00
IS	49.02	35.29	7.84	5.88	14.00	24.00	32.00	30.00
MD	28.00	34.00	30.00	8.00	5.77	17.31	32.69	44.23
RB	15.84	44.55	15.84	23.76	0.00	3.92	18.63	77.45
MG diluvial sand	28.95	31.58	28.95	10.53	6.25	28.12	56.25	9.38
MG aeolian sand	38.24	32.36	23.53	8.82	6.25	37.50	46.87	9.38
MG floodplain sand	2.94	44.12	29.41	23.53	2.70	8.11	27.03	62.16
XM diluvial sand	32.08	35.85	20.75	11.32	5.17	18.97	41.38	34.48
XM floodplain sand	12.24	46.94	30.61	10.20	2.13	6.38	44.68	46.81
XM stabilized dune sand	41.18	29.41	23.53	5.88	8.77	43.86	40.35	7.02
XM mobile dune	58.00	20.00	20.00	2.00	16.98	49.06	32.07	1.89
XQ aeolian sand	54.05	21.62	14.86	9.46	16.42	43.28	37.31	2.99
XQ diluvial sand	35.00	40.00	18.33	6.67	20.34	49.16	28.81	1.69
XQ limnic sand	38.46	29.06	23.08	9.40	2.58	24.14	40.52	32.76
XQ riverbed sand	68.09	15.96	13.83	2.13	15.38	48.35	31.87	4.40

Note: DS, dune sand; IS, interdune sand; MD, muddy desert surface soil; RB, riverbed sand.

In MG profile, aeolian sand exhibited the highest content of circular grains (38.24%) and the best roundness (37.50%). The roundness of floodplain sand was the poorest, with a square particles proportion of 44.12%, and predominance of angular grains (62.16%). In XM profile, both diluvial and floodplain sand showed poor roundness. In contrast, stabilized dune sand

demonstrated better roundness, with a predominant circular (41.18%) and subrounded (43.86%) grains. Mobile dune sand exhibited the best roundness, with over half of them being circular (58.00%), and a substantial proportion of subrounded (49.06%) grains. In XQ profile, the riverbed sand exhibited the best roundness, with a circular grain proportion of 68.09%, and the proportion of subrounded (48.35%) grains exceeding nearly half. The aeolian sand had a slightly lower roundness, with a circular grain content of 54.05%, subrounded grain content of 43.28%. Both diluvial and limnic sand showed poor roundness, but the former was better than the latter.

4.3.2 Surface micro-textures

Typical aeolian features are products of high-energy wind environment, resulting from mutual collision of sand transported by wind. In surface sediment, aeolian features were very prominent on the surface of dune sand (Fig. 10), and the frequencies of each type of features were all above 40% (Figs. 10a and 11). In interdune sand and muddy desert surface soil, there were also a certain number of aeolian features on the surface of quartz sand, with frequencies ranging from 30% to 50%. In MG profile, pockmarked pit and dish-shaped pit on aeolian sand were significantly higher than those on diluvial sand and floodplain sand (Figs. 10b and 12), with frequencies

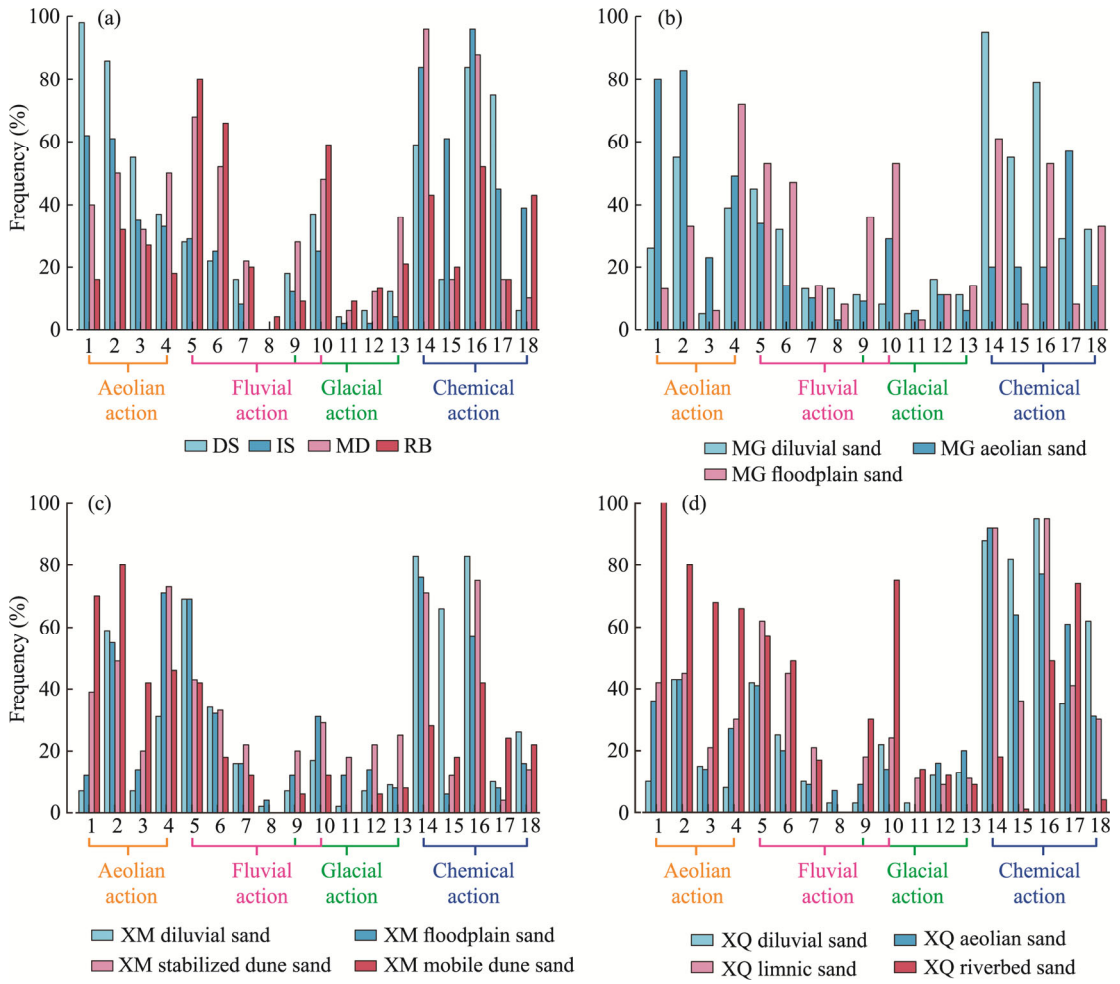

Fig. 10 Frequency of surface micro-texture of quartz sand grains for surface sediment and stratigraphic sediment in study profiles. (a), surface sediment; (b), MG profile; (c), XM profile; (d), XQ profile. 1, pockmarked pit; 2, circular and dish-shaped pit; 3, crescent-shaped impact crater; 4, sinuous ridge; 5, triangular pit; 6, V-shaped pit; 7, straight and bent impact groove; 8, subaqueous polished surface; 9, cleavage plane; 10, conchoidal fracture; 11, stria; 12, deep extrusion pit; 13, triangular and V-shaped flute; 14, siliceous sphere; 15, siliceous scale; 16, siliceous precipitation; 17, crack; 18, etch pit.

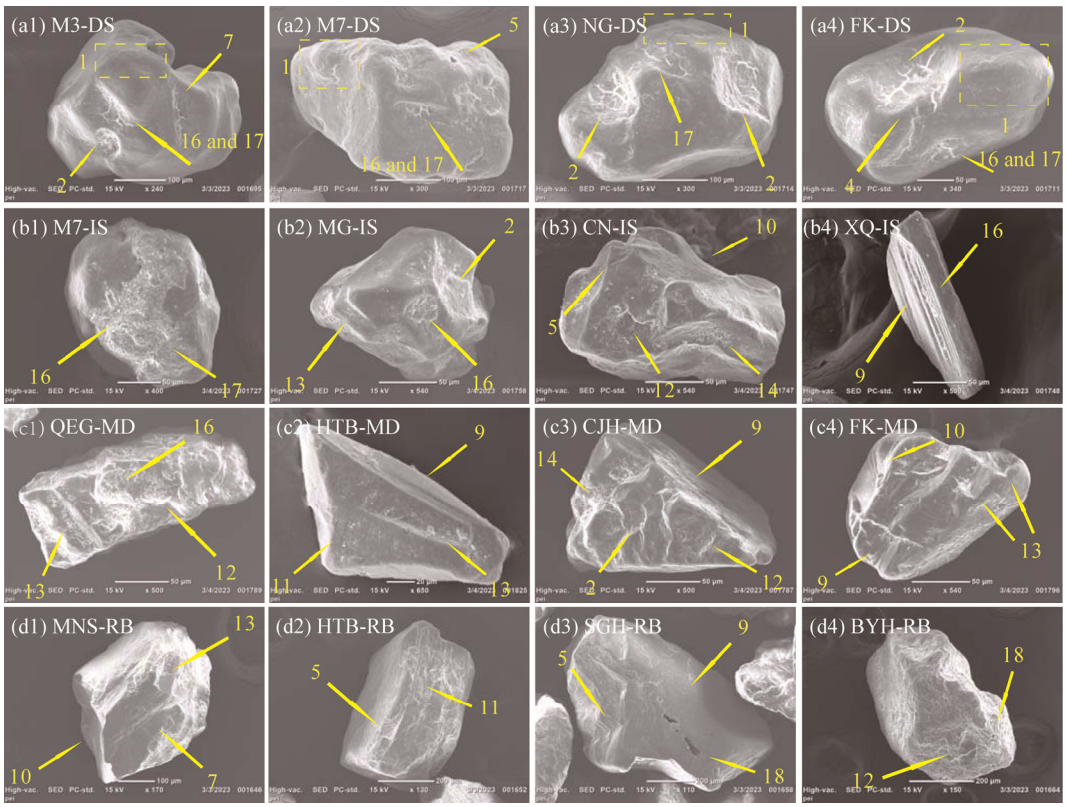

Fig. 11 Surface micro-textures of quartz sand grains for different types of surface sediment in the study area. The micro-texture type corresponding to the number is shown in Figure 10. (a1–a4), DS; (b1–b4), IS; (c1–c4), MD; (d1–d4), RB.

exceeding 80%. In XM profile, aeolian features were focused on stabilized dune sand and mobile dune sand (Figs. 10c and 12), especially on mobile dune sand. In XQ profile, aeolian features on the surface of quartz sand in aeolian layers were not obvious (Figs. 10d and 12), but the riverbed sand showed significant aeolian features, with frequencies approaching 70%, indicating that these sands have been subjected to strong wind action.

Features such as triangular pit, straight impact groove, and conchoidal fracture are products of high-energy fluvial environment, while long-term flow erosion leads to abrasion of sand, forming subaqueous polished surface. In surface sediment, besides the abundant fluvial features on the surface of quartz sand in muddy desert surface soil and riverbed sand, such features were also observed on dune sand and interdune sand at frequencies of about 20% (Figs. 10a and 11). In study profiles, the frequencies of fluvial features on the surface of diluvial sand, floodplain sand, and limnic sand were high, ranging from 30% to 70% (Figs. 10b–d and 12). Similar to dune sand, fluvial features were presented on the surface of aeolian sand in stratigraphic profiles, but frequencies were less than 20%. The fluvial features on riverbed sand in XQ profile were much significant (Fig. 10d). However, these features were fresh and superimposed on aeolian sand (Fig. 12).

In glacial environment, due to strong extrusion, friction, and collision of solid materials, the quartz sand remained some micro-textures such as V-shaped flute, cleavage plane, and conchoidal fracture on its surface. In surface sediment, the glaciated features on surface of quartz sand increased from dune sand, interdune sand, muddy desert surface soil to riverbed sand (Figs. 10a and 11). In MG profile, the sediment with the most glaciated features was floodplain sand, with frequencies between 20% and 50% (Figs. 10b and 12). In XM profile, glaciated features on surface of stabilized dune sand were relatively significant, with frequencies above 20% (Figs. 10c and 12). However, there were few glaciated features on the surface of mobile dune sand, with

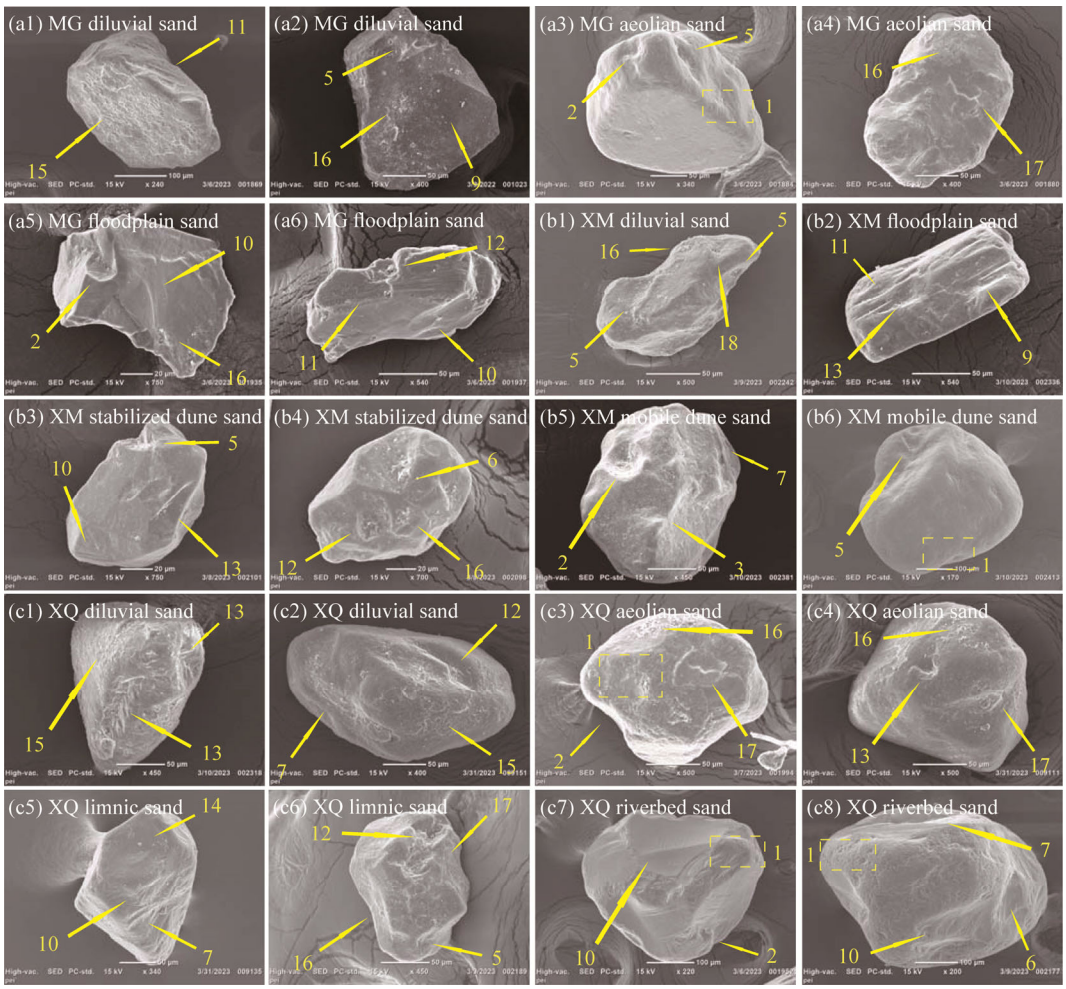

Fig. 12 Surface micro-texture of quartz sand grains for different types of sediment in study profiles. The micro-texture type corresponding to the number is shown in Figure 10. (a1–a6), MG profile; (b1–b6), XM profile; (c1–c8), XQ profile.

frequencies below 10%, indicating potential differences of provenance between the two dune deposits. In XQ profile, glaciated features on the surface of quartz sand were not significant, with frequencies below 20% (Fig. 10d).

In desert environment, intense temperature changes and chemical dissolution usually results in crack, etch pit, and siliceous precipitation on the surface of quartz sand. Among surface sediment, cracks were most developed on the surface of dune sand, with frequencies close to 80% (Figs. 10a and 11). Siliceous precipitation appeared on the surface of quartz sand in interdune sand and muddy desert surface soil, with frequencies exceeding 80%. Etch pits were most common on the surface of riverbed sand, with frequencies exceeding 40%. In study profiles, cracks were most commonly observed on the surface of aeolian sand, with frequencies between 30% and 60% (Figs. 10b–d and 12). Siliceous precipitation on the surface of diluvial sand, floodplain sand, and limnic sand was widespread, with frequencies up to 60%. Etch pits on the surface of quartz sand in all profiles was relatively low, with an average frequency of around 30%.

Overall, whether in surface sediment or stratigraphic sediment, the chemical features on the surface of quartz sand were quite significant, closely related to the relatively good vegetation cover in the Gurbantunggut Desert. The presence of mechanical impact features such as aeolian, fluvial, and glaciated features on particle surface indicated the active exogenic forces in the study area, and sediment had undergone alternating transformation by various exogenic forces.

5 Discussion

5.1 Sedimentary environment reflected by grain size EM and surface micro- texture of quartz sand

Based on the aforementioned analysis, we found that MG profile EM1 and EM2, along with XM profile EM1 and XQ profile EM1, were predominantly presented in diluvial deposits characterized by clay and silt, with a significant proportion of suspension load, akin to muddy desert surface soil. Previous studies have indicated that sediment grain size decreases gradually from upstream to downstream within fluvial dynamic systems, with suspension load mostly comprising clay and fine silt ranging from 10 to 15 mm (Sun et al., 2001). In the alluvial plain at northern piedmont of the Tianshan Mountains, braided rivers experienced a decrease in gradient and flow velocity after emerging from the mountains, eventually flowing into the desert in flood period, resulting in the development of diluvial deposits (Liu et al., 2018). Compared with modern river sand, quartz sand in diluvial deposits exhibited fewer fluvial features and better roundness, reflecting the weak hydrodynamic characteristics of distal reaches near southern margin of the desert (Kang and Dai, 1988; Gao et al., 1995; Wu, 1995). Consequently, such EM represents low-flow suspended deposition in the distal reaches of braided rivers. However, due to weak hydrodynamic force and absence of visible bedding after deposition, such sediment more closely resembles stagnant water deposition (Jin et al., 2019; Yang et al., 2021).

MG profile EM3 and XM profile EM2 were primarily found in floodplain deposits, characterized by wavy bedding and dominated by silt with a significant proportion of suspension load. In the Junggar Basin, influenced by the swing of meandering river, when the flood flow over the alluvial fan downstream of the braided river, suspended and saltatory silts overflow to the convex bank, thereby forming fine-grained sediment on the river overbank (Xie and Yin, 2021). From the characteristics of quartz sand, the roundness of floodplain sand was relatively poor, with significant fluvial features, similar to the quartz sand in muddy desert surface soil and modern riverbed sand, reflecting a mid to high energy flowing water environment. However, the frequent swing of braided rivers at northern piedmont of the Tianshan Mountains led to their gradual transformation into meandering rivers (Tan et al., 2014; Han et al., 2023). Therefore, such EM represents floodplain sediment in the meandering segment downstream of the braided river, with significant changes in water volume after the river merged into the desert, resulting in a considerable proportion of fine-grained components in the sediment (Ren and Wang, 1981).

XQ profile EM2 and EM3 were primarily concentrated within limnic deposits, characterized by predominantly silt and clay, with a mixture of saltation and suspension load. The frequency curves exhibited a broad peak, indicating poor sediment sorting. From sediment structure, both the two EMs appeared gray-green, reflecting an anaerobic reducing environment due to prolonged waterlogging. However, the development of reddish-brown iron-manganese rusty spot within the layer suggested periodic fluctuations in water level (Ren and Wang, 1981). Apart from significant fluvial features, limnic sand also exhibited numerous chemical features, indicating that the sand had been in humid environment for a long time after deposition (Vos et al., 2014). Such characteristics of quartz sand were not only commonly found in muddy desert surface soil and interdune sand but also were prevalent in borehole sediment at southern margin of the desert (Huang and Zhou, 2000; Qian and Wu, 2010). In summary, the two EMs represent lake and marsh wetland deposition in distal reaches of braided rivers with plenty of water.

The stratum hosting MG profile EM4, EM5, and XM profile EM3 exhibited distinct cross-bedding, predominantly composed of sand and silt, displaying good sorting characteristics of aeolian sand. However, compared with modern dune sand, this type of aeolian sand tends to have finer grain size, a higher proportion of suspension load, and insufficiently developed aeolian features on sand surface along with numerous chemical features. Studies have shown that as the mobile dune tend to be stabilized, vegetation coverage increases and fine-grained sand increases significantly (Li and Fan, 2011; Lee et al., 2019). Moreover, during the process of dune stabilization, humidity conditions gradually improved, leading to the development of chemical

features on sand surface. Therefore, such EM likely represents stabilized dune deposition. It is noteworthy that a certain number of fluvial features were observed on aeolian sand surface, indicating that it may have been formed by *in situ* sand accumulation of sediment carried and deposited by rivers at southern margin of the desert (Qian et al., 2003; Zhu et al., 2014; Zhang et al., 2022). XM profile EM4 and EM5 are typical dune sand components, concentrated within the layer of mobile dune deposition, exhibiting characteristics consistent with modern dune sand. These sands had high roundness, significant aeolian features on the surface, but few chemical features, indicating that sand particles were transported by wind in long distance and then deposited in arid environment (Dai, 1988). XQ profile EM4 was predominantly distributed within aeolian sand layers, composed of sand and a small amount of silt. The frequency curve exhibited a bimodal distribution, with saltation load higher than suspension load, and with good sorting. From sediment structure, the aeolian sand layers showed horizontal bedding, displaying the characteristics of sand sheet deposition (Ren and Wang, 1981). However, due to the development of aeolian sand on the diluvial substrate, it was inevitable that the adhesive diluvial sediment mixed with it, resulting in a minor peak and fine tail in the frequency curve (Li et al., 2021). This kind of aeolian sand was moderately rounded, with few aeolian features and a certain number of fluvial features, but the chemical features were significant, indicating that the short transport distance and time, which also reflect the aeolian sand erosion and deposition process of *in situ* sand accumulation (Shi and Xu, 2007; Qian and Wu, 2010).

XQ profile EM5 and EM6 were primarily found within sand layers exhibiting trough cross-bedding, displaying characteristics of riverbed deposition (Ren and Wang, 1981). However, in terms of grain size characteristics, the main particle size of both two EMs ranged from fine sand to medium sand, dominated by saltation load, with sharp peaks and good sorting, indicating aeolian sand characteristics. As previously mentioned, such sand had high roundness, with fluvial features superimposed on aeolian features on its surface, indicating that the two EMs represent aeolian sand modified by fluviation. The higher frequencies of fluvial features reflect abundant river water and strong hydrodynamic force. However, due to the relatively short flow path of the rivers in eastern Tianshan Mountains, the modification of sand by flow was limited, and aeolian features on the sand surface remained prominent. In the downstream of the river in arid desert, due to the interaction between wind and water forces, the transformation of sediment environment for sand grains was widespread. This can manifest as fluvial sand modified by wind action (Garzanti et al., 2022), or as aeolian sand modified by water action (Zhang et al., 2021).

In summary, during Holocene, the desert-oasis transition zone at southern margin of the Gurbantunggut Desert mainly developed a stratigraphic sequence alternating between braided river deposits and aeolian deposits. Influenced by climate, terrain, and variations in exogenic forces, southern margin of the desert exhibited the development of braided river deposits, including low-energy suspended diluvial deposits, meandering channel floodplain deposits, limnic deposits, as well as riverbed deposits. Additionally, aeolian deposits, including sand sheet deposits, stabilized dune deposits, and mobile dune deposits were prevalent. Considering the chronology of stratigraphy, from 11.8 to 10.2 ka, rivers in southeastern margin of the desert had high discharge and strong hydropower. Frequent meandering of braided rivers led to the mixing of aeolian sand into river channel, forming riverbed deposits. At the same time, glacial meltwater deposits were developed in the interdune of southeastern margin of the desert (Li and Fan, 2011), and thick alluvial clay layer was developed in HG profile (Zong et al., 2022). Ebinur Lake also appeared high water level (Wu et al., 2003), indicating that alluvial deposits were prevalent on the margin of the desert at this stage. From 10.2 to 6.0 ka, braided rivers had abundant discharge, and end of the river may have developed shallow wetland in low-lying areas at the margin of the desert, resulting in limnic deposits. The increase of regional humidity during this period was also recorded by other sedimentary sequences at the margin of the desert. FK profile was dominated by silty clay deposits (Zong et al., 2022). Clay mineral deposits were developed in the lower reaches of the Manas River, China (Shi et al., 2007). SFC profile in the lower reaches of the Hutubi River developed riverbed deposits and lacustrine deposits (Tan et al., 2023), and the water

level of the Ebinur Lake was also gradually rising (Wu et al., 1996). Since 6.0 ka, hydropower of braided rivers at southern margin of the desert gradually weakened. This period witnessed the development of meandering channel floodplain deposits followed by low-energy suspended diluvial deposits in terminal river reaches. Meanwhile, intermittent enhancement of aeolian activity led to desert encroachment. Influenced by the underlying topography and surface substrate, various aeolian deposits, including aeolian sand sheets, stabilized dunes, and mobile dunes, emerged. These aeolian deposits interacted and overlapped with river deposits, forming a complex alluvial-aeolian composite sequence. During this time, MNS profile in the southwest of the desert recorded the alternating changes of aeolian-alluvial process (Zong et al., 2022), and SFC profile reflected the interaction between river alluvial and aeolian accumulation (Tan et al., 2023). In addition, the Dongdaohaizi Lake (Yan et al., 2004; Li et al., 2005; Ma et al., 2005) and the Ebinur Lake (Wu et al., 1996) also experienced frequent variations in water level, reflecting the fluctuations of aeolian and alluvial processes at the margin of the desert in mid to late Holocene.

5.2 Provenance indication of grain size and quartz sand surface micro-texture

Previous studies have shown that sand provenance of the Gurbantunggut Desert is mainly the clastic materials produced by the weathering and erosion of rocks in surrounding mountains, as well as the contribution of fluvial and lacustrine sediment at the margin of the desert and the underlying sand in the basin (Zhu et al., 1980; Qian et al., 2001; Qian et al., 2003; Shi et al., 2006; Zhu et al., 2014; Huang et al., 2018; Zhang et al., 2022). As southern margin of the desert is located at the convergence zone of wind and water forces, both exogenic forces exert a certain degree of modification on the debris from surrounding mountains, making the sediment source more complex compared with other areas of the desert. In provenance analysis of desert sediment, the abrasion of sand during transport by different exogenic forces often leads to differences in their grain size characteristics, making them distinct from the sediment in the source area (Jerolmack et al., 2011). Relying solely on grain size analysis may not be sufficient to accurately determine the sand provenance (Gao et al., 2022b). However, features such as roundness and surface micro-textures of quartz sand can provide important references for provenance discrimination (Vos et al., 2014). Therefore, this study, based on grain size analysis, combines characteristics of quartz sand to explore the provenance of sediment at southern margin of the desert.

Alluvial deposits at southern margin of the desert were primarily formed by alluviation from rivers originating from northern piedmont of the Tianshan Mountains and seasonal precipitation. Potential provenance of this material could be the debris produced by glacial erosion and abrasion, as well as frost weathering in the Tianshan Mountains. In surface sediment, the quartz sand in muddy desert surface soil and riverbed sand exhibited poor roundness, with numerous prominent fluvial features and significant glaciated features. These characteristics indicated that debris from the Tianshan Mountains was the main provenance of modern alluvial sand at southern margin of the desert. Stratigraphic sediment, including diluvial sand, floodplain sand, and limnic sand, displayed similar features, suggesting that weathered debris from the Tianshan Mountains played a crucial role in supplying material to the alluvial deposits at southern margin of the desert during Holocene. The interaction between rivers and dunes at southern margin of the Gurbantunggut Desert represents a unique pattern, namely scattered by dune- and field-parallel drainage (Li et al., 2019). Various rivers originating from northern slopes of the Tianshan Mountains can transport debris generated by glacial abrasion and frost weathering without interfering with each other, depositing sand materials at southern margin of the desert. Furthermore, during Holocene, there had been no significant tectonic alteration in the Junggar Basin, confirming that alluvial deposits at southern margin of the desert consistently originated from the Tianshan Mountains.

Grain size of surface sand in the Gurbantunggut Desert gradually decreases from northwest to southeast, with the finest sand observed in the south of the desert, primarily composed of very fine and fine sand, and exhibiting poor roundness (Qian and Wu, 2010; Zhao, 2020; Zhu et al.,

2021; Gao et al., 2022a). However, the results of this study showed that in modern dune sand at southern margin of the desert, fine sand and medium sand were predominant. This was similar to the characteristics of surface sand in central desert. Additionally, there were clear aeolian features on the sand, with good roundness. This result suggested that under the conditions of strong wind or dust storm, sand from the interior of the desert may be transported and subsequently accumulated at southern margin (Pye, 1987). In the stratigraphic profiles, sand layer at bottom of XQ profile was aeolian sand modified by fluviation, consistent with the grain size characteristics of mobile dune sand in XM profile. Predominant grain size components were fine sand and medium sand, with well-rounded quartz sand and significant aeolian features on the surface. Therefore, the source area may also be the interior of the desert. Aeolian sand of MG profile, stabilized dune sand of XM profile, and aeolian sand of XQ profile exhibited finer grain size, similar to modern muddy desert surface soil and interdune sand. They all showed a higher content of silt, along with poor roundness of quartz sand, and fluvial features and glaciated features contribute significantly. These characteristics collectively reflect the proximal nature of such aeolian sand (Pye, 1987; Qian et al., 2000; Vos et al., 2014), indicating that they may primarily originated from the widespread alluvial deposits in the south of the desert. Current studies also suggested that fluvial and lacustrine deposits in south of the desert served as a "transit station" for the transfer of weathered debris from the Tianshan Mountains. After being transported by wind erosion, they provided sand provenance for the development of dunes at southern margin of the desert (Tursun et al., 2022; Zhang et al., 2022). Ultimately, regardless of how the sands were processed and modified, their provenance was still the debris formed by glacier erosion and abrasion, and frost weathering from the Tianshan Mountains. However, recent study has shown that there is spatial heterogeneity in sand provenance of the Gurbantunggut Desert. In spring and winter, when dust storms occur frequently, weathered debris from the Altay Mountains can be transported to the central and eastern parts of the desert with prevailing winds, and the sand in western part of the desert comes from the Junggar Basin (Li et al., 2024). Under the action of strong wind, the southern part of the desert, which is located in the downwind direction of prevailing winds, may be affected by sand input. Therefore, the contribution of weathered debris of the mountains around the Junggar Basin to the development of dunes in southern margin of the desert remains to be further studied.

6 Conclusions

Based on the analysis of OSL chronology, grain size, quartz sand morphology, and surface micro-texture, we explored the sediment environmental change and sand provenance in southern margin of the Gurbantunggut Desert in Holocene. Around 11.8 to 10.2 ka, frequent swings of braided river on southern margin of the desert led to the entrainment of aeolian sand along the river bank, forming riverbed deposits. From 10.2 to 6.0 ka, the braided river exhibited abundant water flow, resulting in the inflow of tail water into the desert fringe, forming limnic deposits. Since 6.0 ka, the water in the braided river diminished, leading to the development of meandering floodplain deposits and low-flow suspended diluvial deposits in the tail water section. During the periods of enhanced aeolian activity, the desert encroached southward, and aeolian deposits formed on the substrates of river deposits, and overlapping with them. In Holocene, the alluvial deposits at southern margin of the desert had a relatively stable provenance, consistently composed of debris transported by river flow and intermittent floods from the Tianshan Mountains. Aeolian sand was primarily supplied from proximal source, formed by *in situ* deposition of fluvial and lacustrine sediment transported by wind erosion in southern desert. Additionally, sand from the interior of the desert may underwent transportation on a desert scale via strong wind such as dust storm, contributing to the development of dunes at southern margin of the desert. The results provide reference for studying the formation and evolution of the Gurbantunggut Desert and preventing desertification in the future.

Conflict of interest

The authors declare that they have no known competing financial interests or personal relationships that could have appeared to influence the work reported in this paper.

Acknowledgements

This research was funded by the National Natural Science Foundation of China (42071011) and the 2023 Annual Postgraduate Research and Innovation Foundation of Fujian Normal University, China.

Author contributions

Conceptualization: MA Yunqiang; Data curation: MA Yunqiang, TAN Dianjia, ZOU Xiaojun, TAO Tonglian; Methodology: MA Yunqiang, LI Zhizhong; Formal analysis: MA Yunqiang, TAN Dianjia, ZOU Xiaojun; Software: TAO Tonglian; Writing-original draft preparation: MA Yunqiang; Writing-review and editing: MA Yunqiang, LI Zhizhong, TAN Dianjia; Funding acquisition: LI Zhizhong. All authors approved the manuscript.

References

Aitken M J. 1998. An Introduction to Optical Dating. Oxford: Oxford University Press.

Chen X. 2010. Natural Geography of Arid Areas in China. Beijing: Science Press. (in Chinese)

Chen Z P. 1963. Basic Features of Gurbantunggut Desert in Junggar Basin. Beijing: Science Press. (in Chinese)

Dai F N. 1988. The relationship between sedimentary environments and features of surface textures of quartz sand in sand dunes of desert area in northern China. Journal of Arid Land Resources and Environment, 2(2): 25–35. (in Chinese)

Folk R L, Ward W C. 1957. Brazos river bar: A study in the significance of grain size parameters. Journal of Sedimentary Research, 27(1): 3–26.

Gao C H, Mu G J, Yan S, et al. 1995. Features of surface micro-textures of quartz sand grains in the hinterland of the Taklimakan Desert and their environmental significance. Geological Review, 41(2): 152–158. (in Chinese)

Gao C, Dong Z B, Nan W G, et al. 2022a. Physicochemical characteristics and sedimentary environment of honeycomb dunes in Gurbantunggut Desert. Journal of Desert Research, 42(2): 14–24. (in Chinese)

Gao W T, Wang B, Peng J, et al. 2022b. Spatial distribution of granularity parameter and provenance indication of aeolian deposits on the southern margin of Tengger Desert. Research of Soil and Water Conservation, 29(6): 129–137. (in Chinese)

Garzanti E, Pastore G, Stone A, et al. 2022. Provenance of Kalahari Sand: Paleoweathering and recycling in a linked fluvial-aeolian system. Earth Science Reviews, 224: 103867, doi: 10.1016/j.earscirev.2021.103867.

Goudie A S. 2002. Great Warm Deserts of the World: Landscapes and Evolution. Oxford: Oxford University Press.

Goudie A S, Middleton N J. 2006. Desert Dust in the Global System. Heidelberg: Springer.

Han Z L, Jianatayi D, Yao Z Q, et al. 2023. Analysis of sedimentary characteristics of braided river to meandering river: Taking Toutunhe formation on the eastern margin of Fukang Sag as an example. Fault-Block Oil & Gas Field, 30(3): 434–440. (in Chinese)

Huang Q. 1996. Environmental changes in the Gurbantunggut Desert since the Late Pleistocene. MSc Thesis. Urumqi: Xinjiang Institute of Ecology and Geography, Chinese Academy of Sciences. (in Chinese)

Huang Q, Zhou X J. 2000. The climate environment changes in the south of Gurbantunggut Desert since 80 ka BP. Arid Land Geography, 23(1): 55–60. (in Chinese)

Huang Y Z, Chen X L, Cheng L Q, et al. 2018. REE characteristics and its provenance implication of surface sediments in the Junggar Basin. Quaternary Sciences, 38(6): 1325–1335. (in Chinese)

Jerolmack D, Reitz M, Martin R. 2011. Sorting out abrasion in a gypsum dune field. Journal of Geophysical Research, 116(2): 1–15.

Jin J, Liu D W, Ji Y L, et al. 2019. Research on lithofacies types, cause mechanisms and distribution of a gravel braided river alluvial fan: A case study of the modern Poplar River alluvial fan, northwestern Junggar Basin. Acta Sedimentologica Sinica, 37(2): 254–267. (in Chinese)

Kang D G, Dai F N. 1988. Features of quartz grains surface textures in the Keriya River, Taklimakan Desert. Journal of Desert Research, 8(4): 46–51. (in Chinese)

Krinsley D H, Doornkamp J C. 1973. Atlas of Quartz Sand Surface Textures. Cambridge: Cambridge University Press.

Lai Z P, Ou X J. 2013. Basic procedures of optically stimulated luminescence (OSL) dating. Progress of Geography, 32(5): 683–693. (in Chinese)

Lancaster N. 1995. Geomorphology of Desert Dunes. Cambridge: Cambridge University Press.

Lee D B, Ferdowsi B, Jerolmack D J. 2019. The imprint of vegetation on desert dune dynamics. Geophysical Research Letters, 46(21): 12041–12048.

Li B F, Feng Q, Li Z J, et al. 2024. Provenance of surface dune sands in the Gurbantunggut Desert, northwestern China: Qualitative and quantitative assessment using geochemical fingerprinting. Geomorphology, 452: 109115, doi: 10.1016/j.geomorph.2024.109115.

Li J Y, Qu X, Dong Z B, et al. 2021. Contribution of underlying terrain to sand dunes: Evidence from the Qaidam Basin, Northwest China. Journal of Arid Land, 13(12): 1215–1229.

Li S F, Yan S, Kong Z C, et al. 2005. Diatom records and environmental changes of the Dongdaohaizi area in Urumqi, Xinjiang. Arid Land Geography, 28(1): 81–87. (in Chinese)

Li S H, Fan A C. 2011. OSL chronology of sand deposits and climate change of last 18 ka in Gurbantunggut Desert, Northwest China. Journal of Quaternary Science, 26(8): 813–818.

Li X M, Yan P, Liu B L. 2020. Geomorphological classification of aeolian-fluvial interactions in the desert region of north China. Journal of Arid Environments, 172: 104021, doi: 10.1016/j.jaridenv.2019.104021.

Liu D W, Ji Y L, Gao C L, et al. 2018. Microfacies and sedimentary models of gravelly braided river alluvial fan: A case study of modern Baiyanghe river alluvial fan in northwestern margin of Junggar Basin. Journal of Paleogeography, 20(3): 435–451. (in Chinese)

Liu Z Y. 2022. Sandy landform and development environment of Gurbantunggut Desert. PhD Dissertation. Xi'an: Shaanxi Normal University, 26–28. (in Chinese)

Ma N N, Mu G J, Yan S. 2005. Discussion and analysis on sediment source of Dongdaohaizi B section in Urumqi since middle Holocene. Arid Land Geography, 28(2): 188–193. (in Chinese)

Murray A S, Wintle A G. 2000. Luminescence dating of quartz using an improved single-aliquot regenerative-dose protocol. Radiation Measurements, 32(1): 57–73.

Parsons A J, Abrahams A D. 2009. Geomorphology of Desert Environments. Dordrecht: Springer.

Paterson G A, Heslop D. 2015. New methods for unmixing sediment grain size date. Geochemistry, Geophysics, Geosystems, 16(2): 4494–4506.

Powers M C. 1953. A new roundness scale for sedimentary particles. Journal of Sedimentary Petrology, 23(2): 117–119.

Prescott J R, Hutton J T. 1994. Cosmic ray contributions to dose rates for luminescence and ESR dating: Large depths and long-term time variations. Radiation Measurements, 23(2–3): 497–500.

Pye K. 1987. Aeolian Dust and Dust Deposits. London: Academic Press.

Pye K, Tsoar H. 2009. Aeolian Sand and Sand Dunes. Berlin: Springer.

Qian Y B, Zhou X J, Wu Z N. 2000. Study on the grain size's characteristics of the sand materials in the Junggar Basin. Arid Zone Research, 17(2): 34–41. (in Chinese)

Qian Y B, Zhou X J, Li C S, et al. 2001. Multi-sources of sand minerals for the desert in the Junggar Basin. Journal of Desert Research, 21(2): 182–187. (in Chinese)

Qian Y B, Zhou X J, Wu Z N, et al. 2003. Multi-sources of desert sands for the Jungger Basin. Journal of Arid Environments, 53(2): 241–256.

Qian Y B, Wu Z N. 2010. Environments of Gurbantunggut Desert. Beijing: Science Press. (in Chinese)

Ren M D, Wang N L. 1981. Generality to Modern Sedimentary Environments. Beijing: Science Press. (in Chinese)

Robins L, Greenbaum N, Yu L P, et al. 2021. High-resolution portable OSL analysis of vegetated linear dune construction in the margins of the northwestern Negev dunefield (Israel) during the Late Quaternary. Aeolian Research, 50: 100680, doi: 10.1016/j.aeolia.2021.100680.

Shi X M, Li Y L, Yang J C. 2007. Environmental significance and clay mineral characteristics of Mogu Lake sediment of Manas River. Arid Land Geography, 30(1): 84–88. (in Chinese)

Shi X M, Xu S N. 2007. Environmental significance and characteristics of sands of Manas River lacustrine plain. Research of Soil and Water Conservation, 14(6): 157–159. (in Chinese)

Shi Z T, Song Y G, An Z S. 2006. Evolution of Gurbantunggut Desert recorded by Tianshan Loess. Journal of Desert Research, 26(5): 675–679. (in Chinese)

Stokes S, Bailey R M, Fedoroff N, et al. 2004. Optical dating of aeolian dynamism on the west African Sahelian margin. Geomorphology, 59(1–4): 281–291.

Sun D H, An Z S, Su R X, et al. 2001. Mathematical method for separation of grain size components of sediments in paleoenvironment and its application. Progress in Natural Science, 11(3): 269–276. (in Chinese)

Tan C P, Yu X H, Li S L, et al. 2014. Discussion on the model of braided river transform to meandering river: As an example of Toutunhe formation in southern Junggar Basin. Acta Sedimentologica Sinica, 32(3): 450–458. (in Chinese)

Tan D J, Ma Y Q, Li Z Z, et al. 2023. Environmental evolution of middle-late Holocene verified by sedimentary evidences in the alluvial plain in the northern foothills of the Tianshan Mountains, China. Mountain Research, 41(3): 307–321. (in

Chinese)

Team Northern Shannxi of Chengdu Institute of Geology (TNSCIG). 1978. Grain Size Analysis of Sedimentary Rocks and Its Application. Beijing: Science Press. (in Chinese)

Tursun D, Zhang F, Wu F, et al. 2022. Geochemical characterization of major elements in Gurbantunggut Desert sediments, northwestern China and their regional variations. Aeolian Research, 57: 100802, doi: 10.1016/j.aeolia.2022.100802.

Vos K, Vandenberghe N, Elsen J. 2014. Surface textural analysis of quartz grains by scanning electron microscopy (SEM): From sample preparation to environmental interpretation. Earth Science Reviews, 128: 93–104.

Wang X L, Lu Y C, Li X N. 2005. Luminescence dating of fine- grained quartz in Chinese loess-simplified multiple aliquot regenerative-dose (MAR) protocol. Seismology Geology, 27(4): 615–622. (in Chinese)

Wintle A G, Murray A S. 2006. A review of quartz optically stimulated luminescence characteristics and their relevance in single-aliquot regeneration dating protocols. Radiation Measurements, 41(4): 369–391.

Wu J L, Wang S M, Wang H D. 1996. Characters of the evolution of climate and environment of Holocene in Aibi Lake Basin in Xinjiang. Oceanologia et Limnologia Sinica, 27(5): 524–530. (in Chinese)

Wu J L, Shen J, Wang S M, et al. 2003. Characteristics of early Holocene climate and environment recorded by lake sediments in Ebinur Lake area, Xinjiang. Science China Earth Sciences, 33(6): 569–575. (in Chinese)

Wu Z. 1962. The Basic Characteristics of Desert Landform Development in Junggar Basin. Beijing: Science Press. (in Chinese)

Wu Z. 1995. A comparative study of the surface texture of quartz sand in inland deserts than in coastal dunes, China. Journal of Desert Research, 15(3): 201–206. (in Chinese)

Wu Z. 2009. Chinese Desert and Its Governance. Beijing: Science Press. (in Chinese)

Xinjiang Expedition of Chinese Academy of Sciences (XECAS). 1978. Xinjiang Landform. Beijing: Science Press. (in Chinese)

Yan S, Li S F, Kong Z C, et al. 2004. The pollen analyses and environment changes of the Dongdaohaizi area in Urumqi, Xinjiang. Quaternary Sciences, 24(4): 463–468. (in Chinese)

Yang X P, Karl T R, Frank L, et al. 2004. The evolution of dry lands in northern China and in the Republic of Mongolia since the Last Glacial Maximum. Quaternary International, 118–119: 69–85.

Yang X P, Li H W, Conacher A. 2012. Large-scale controls on the development of sand seas in northern China. Quaternary International, 250: 74–83.

Yang X P, Eitel B. 2016. Understanding the interactions between climate change, landscape evolution, surface processes and tectonics in the Earth system: What can the studies of Chinese deserts contribute? Acta Geologica Sinica, 90(4): 1444–1454.

Yang X P, Du J H, Liang P, et al. 2021. Paleoenvironmental changes in the central part of the Taklamakan Desert, northwestern China since the late Pleistocene. Chinese Science Bulletin, 66(24): 3205–3218.

Yin H Z. 1978. The relationship between the tectonics and geomorphology in the Junggar Basin. Arid Land Geography, 10(4): 13–21. (in Chinese)

Zhang F, Xia Q Q, Dilibaier T, et al. 2021. Holocene hydrology and environment changes in the Keriya River Delta in 13.8–2.3 ka in Taklimakan Desert: Inferred from the stratigraphy. Arid Land Geography, 44(1): 178–187. (in Chinese)

Zhang Z C, Liang A M, Dong Z B, et al. 2022. Sand provenance in the Gurbantunggut Desert, northern China. Catena, 214: 106242, doi: 10.1016/j.catena.2022.106242.

Zhao J. 2020. Study on the characteristics of aeolian sediments in Gurbantunggut Desert. MSc Thesis. Xi'an: Shaanxi Normal University. (in Chinese)

Zhu B Q, Yu J J, Qin X G, et al. 2014. Formation and evolution of sand desert in Xinjiang, Northwest China: Provenance of desert sands. Journal of Geographical Sciences, 24(1): 177–190.

Zhu C M, Dong Z B, Liu Z Y, et al. 2021. Grain size and micro-morphology characteristics of the surface sediments of dendritic sand dunes in the Gurbantunggut Desert. Journal of Desert Research, 41(2): 9–18. (in Chinese)

Zhu Z D, Wu Z, Liu S. 1980. Generality to Chinese Desert. Beijing: Science Press. (in Chinese)

Zong H R, Fu X, Li Z J, et al. 2022. Multi-method pIRIR dating of sedimentary sequences at the southern edge of the Gurbantunggut Desert, NW China and its paleoenvironmental implications. Quaternary Geochronology, 70: 101300, doi: 10.1016/j.quageo.2022.101300.